Metamaterial-Integrated Microstrip Patch Antenna for Enhanced Near-Field Material Detection

Dissertation submitted in partial fulfillment of the requirements
for the award of the degree of

Dual Degree (B.Tech + M.Tech.)

by

Pullabhotla Bhuvana Chandra

(Roll No. 200070063)

Supervisor:

Prof. Jayanta Mukherjee

Department of Electrical Engineering

INDIAN INSTITUTE OF TECHNOLOGY BOMBAY

Mumbai - 400076, India

June, 2025

Dissertation Approval

This dissertation entitled **Metamaterial-Integrated Microstrip Patch Antenna for Enhanced Near-Field Material Detection** by **Pullabhotla Bhuvana Chandra**, Roll No. 200070063, is approved for the degree of **Dual Degree (B.Tech + M.Tech.)** from the Indian Institute of Technology Bombay.

Digital Signature
Kushal Rajanikant Tuekley
(i16107)
26-Jun-25 05:34:00 PM

Prof. Kushal Tuckley
(Examiner 1)

Digital Signature
Biplab Banerjee (10001772)
26-Jun-25 09:20:32 PM

Prof. Biplab Banerjee
(Examiner 2)

Digital Signature
Jayanta Mukherjee (i07005)
26-Jun-25 09:14:53 AM

Prof. Jayanta Mukherjee
(Supervisor)

Digital Signature
Kushal Rajanikant Tuekley
(i16107)
26-Jun-25 05:34:46 PM

Prof. Kushal Tuckley
(Chairman)

Defence Date: 23-06-2025

Place: IIT Bombay

Certificate

This is to certify that the dissertation entitled **"Metamaterial-Integrated Microstrip Patch Antenna for Enhanced Near-Field Material Detection"**, submitted by **Pullabhotla Bhuvana Chandra** to the Indian Institute of Technology Bombay, for the award of the degree of **Dual Degree (B.Tech + M.Tech.)** in Electrical Engineering, is a record of the original, bona fide research work carried out by him under our supervision and guidance. The dissertation has reached the standards fulfilling the requirements of the regulations related to the award of the degree.

The results contained in this dissertation have not been submitted in part or in full to any other University or Institute for the award of any degree or diploma to the best of our knowledge.

Digital Signature
Jayanta Mukherjee (i07005)
26-Jun-25 10:07:00 AM

. . . . . .

Prof. Jayanta Mukherjee
Department of Electrical Engineering,
Indian Institute of Technology Bombay.

Declaration

I declare that this written submission represents my ideas in my own words. Where others' ideas and words have been included, I have adequately cited and referenced the original source. I declare that I have adhered to all principles of academic honesty and integrity and have not misrepresented or fabricated, or falsified any idea/data/fact/source in my submission. I understand that any violation of the above will cause disciplinary action by the Institute and can also evoke penal action from the source which has thus not been properly cited or from whom proper permission has not been taken when needed.

Digital Signature
Pullabhotla Bhuvana Chandra
(200070063)
26-Jun-25 08:12:38 AM

. . . . . .

Pullabhotla Bhuvana Chandra
Roll No.: 200070063
Date: 23-06-2025
Place: IIT Bombay

Abstract

This thesis focuses on the design and development of a metamaterial-integrated microstrip patch antenna intended for the non-invasive characterization of materials placed near its surface. The primary objective is to achieve a highly sensitive antenna structure capable of detecting small variations in material properties, particularly for materials of very small size, by observing changes in the antenna's S-parameters, resonant frequency, and bandwidth. Multiple antenna designs were modeled and analyzed using simulation tools and one of the most promising configurations was fabricated for experimental testing. The fabricated antenna was subjected to a range of test materials to evaluate its response, with detailed measurements recorded under controlled conditions.

Using the properties of the metamaterial, the antenna exhibited an enhanced electromagnetic interaction with nearby materials, thus improving its sensitivity. The data collected were analyzed to assess material characteristics such as dielectric nature, conductivity, and classification into metallic or nonmetallic categories. Furthermore, when unknown samples were introduced, their electromagnetic response was compared with previously obtained data to infer potential material properties, highlighting the antenna's capability as a reusable and reference-based sensor. The methodology and design approach were inspired by recent advances in metamaterial-based sensor research, particularly the work of [1] on biological material detection. The results of this work demonstrate the feasibility of using compact microstrip antennas as efficient, passive, and cost-effective sensors for material detection in biomedical, industrial, and environmental applications.

Contents

List of Figures

List of Tables

Chapter 1

Introduction

1.1 Introduction

Microstrip patch antennas have become increasingly important in sensing applications due to their compact structure, ease of integration, and low-profile design. When enhanced with metamaterial structures, these antennas exhibit improved sensitivity to environmental changes, particularly in their electromagnetic response. This enhanced capability enables the detection and characterization of materials placed in proximity to the antenna surface.

The primary motivation behind this research is to utilize the metamaterial properties of a microstrip antenna to detect small-sized material samples based on changes in the antenna's S-parameters, resonant frequency, and bandwidth. Using Ansys HFSS, a leading 3D full-wave electromagnetic simulator, various antenna configurations were designed and evaluated for their sensitivity to nearby materials. While multiple designs were explored in the simulation phase, a single optimized antenna was fabricated to verify that the simulated and measured resonant frequencies align, ensuring the design's practical feasibility.

This thesis builds on concepts from recent literature, including the work by Singh et al. (2024), which showcases the use of metamaterial-loaded patch antennas for biological material characterization. However, unlike experimental studies, the material sensitivity analysis in this work is performed solely through simulation, laying the groundwork for future fabrication and real-world testing in sensing domains.

1.2 Problem Statement

Conventional microstrip antennas often lack the sensitivity to detect small-sized materials—especially those with low dielectric contrast—placed near their surface. This limitation makes it difficult to use such antennas for applications that require accurate and non-invasive detection. The problem addressed in this study is to design a compact antenna, integrated with metamaterials, that can detect minute changes in material properties based on electromagnetic variations observed through simulation.

1.3 Need of the Study

There is a growing demand for passive, compact, and highly sensitive sensors in biomedical, industrial, and environmental applications. Antennas with enhanced material sensitivity can play a crucial role in enabling non-contact, real-time detection systems. This study aims to address this need by developing a simulation-based framework for material detection using a metamaterial-loaded antenna.

1.4 Study Objective

The main objectives of the study are:

- Design a metamaterial-integrated microstrip patch antenna with high sensitivity to nearby materials.
- Simulate and evaluate various antenna geometries using HFSS.
- Observe the changes in the S-parameters and the resonant frequency due to the presence of different material samples.
- To fabricate the optimal antenna design and validate its resonant frequency experimentally.
- To provide a reference framework for identifying unknown materials based on simulation results.

1.5 Dissertation Organization

This dissertation consists of 6 chapters, including the present chapter (Chapter 1) which introduces the research topic, defines the problem, and outlines the objectives.

Chapter 2 presents a detailed literature survey on metamaterial antennas and their sensing applications. Chapter 3 explains the methodology and simulation procedure used to achieve the objectives of the study.f the study. Chapter 4 discusses the design variations, simulation trials, and fabrication of the selected antenna. Chapter 5 provides the results and interpretations based on the simulations and the prototype fabricated. Chapter 6 concludes the study by summarizing key findings and proposing future directions.

Chapter 2

Literature Review

2.1 Metamaterial Properties in Antennas

Metamaterials are artificially engineered structures designed to control electromagnetic wave propagation in ways that conventional materials cannot. These materials can exhibit negative values of permittivity (ε) and permeability (μ), enabling exotic phenomena such as negative refractive index and backward wave propagation. Such behaviors are highly advantageous in antenna design, where they allow for miniaturization, gain enhancement, and high field localization.

In particular, microstrip patch antennas benefit significantly from metamaterial integration. As seen in multiple studies, metamaterial structures such as electromagnetic band gaps (EBG), artificial magnetic conductors (AMC), and split ring resonators (SRRs) can modify the effective electromagnetic behavior around the patch. These structures enhance the radiation efficiency, sensitivity to nearby materials, and allow operation at lower physical dimensions for the same frequency band.

2.2 Analysis of Split Ring Resonators in Miniaturized Microstrip Patch Antennas

In the paper titled *"Effect of Single Complimentary Split Ring Resonator Structure on Microstrip Patch Antenna Design"* by [3], a comparative study is conducted between conventional patch antennas and antennas integrated with complementary split ring resonators (CSRRs). A typical microstrip patch antenna is limited in size due to its dependence on half-wavelength resonance. This restricts its application in compact devices where size is a constraint.

The authors introduce single CSRRs—square, circular, triangular, and rhombic—into the center of a 2.4 GHz microstrip antenna and analyze changes in performance using CST simulations. The square CSRR design achieves the highest gain of 6.508 dB, compared to 6.334 dB for the regular patch antenna, and shifts the resonant frequency slightly to 2.414 GHz. This gain improvement and frequency shift occur without changing the physical size of the patch, demonstrating effective miniaturization.

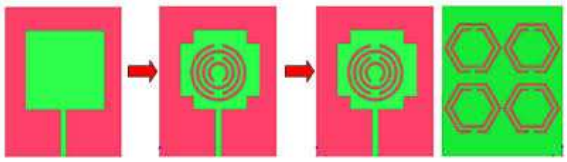

FIGURE 2.1: Modifying the patch with SRR ([2])

The inclusion of the CSRR introduces an artificial LC resonance that modifies the current distribution and local electromagnetic properties. The study further investigates CSRR positioning and finds that placing the resonator 6.25 mm off-center results in an improved gain of 6.577 dB. These results confirm that even a single metamaterial element can significantly enhance antenna performance,

providing a pathway to designing compact, high-sensitivity antennas suitable for material detection.

2.3 Metamaterial-Based Sensing in Patch Antennas

The paper by [1] proposes a metamaterial-loaded patch antenna designed for non-invasive characterization of biological materials. Operating at 12.12 GHz, the antenna incorporates square split ring resonators (SSRRs) around the patch and achieves a return loss (S_{11}) of -42.01 dB. This demonstrates strong resonance and sensitivity.

A significant contribution of this work is the development of a simulation dataset of over 1000 samples with varying dielectric properties. Using these results, a machine learning regression model is built in Python to predict the permittivity and conductivity of unknown samples based on S-parameters. The model is integrated into a user-friendly GUI, turning the antenna into a smart sensing platform.

The antenna structure also includes a cavity-backed design and optimal sample placement at a 4 mm air gap, which improves field interaction. The authors also test biological material detection, including the dielectric changes in BSA (Bovine Serum Albumin) due to denaturation in urea.

This paper sets a benchmark for using patch antennas as sensors, demonstrating how metamaterial loading combined with machine learning and simulation data transforms a passive antenna into an intelligent, real-time, non-contact sensing tool. The present thesis builds on this idea, adapting and modifying the antenna design using alternative metamaterial geometries for material detection.

2.4 Performance Enhancement Using FSS Structures in Planar Antennas

Frequency Selective Surfaces (FSS) are periodic arrays of conductive elements that behave as spatial filters for electromagnetic waves. Depending on their geometry and orientation, FSS can function as either band-pass or band-stop filters. When integrated with planar patch antennas, they can significantly enhance the radiation performance, reduce surface wave losses, and improve bandwidth, gain, and return loss characteristics.

In the study by [4], a planar patch antenna was enhanced by introducing an FSS made of **fractal cross-shaped elements**. The FSS was positioned at various heights above the antenna and tested for different configurations. The optimal design, with the FSS placed at a height of 21.1 mm, yielded a maximum return loss of -52.96 dB at a resonant frequency of 6.7 GHz. This indicates excellent impedance matching and reduced backscattering. Moreover, bandwidth improvements were also observed when the FSS was placed closer (at 6.1 mm), reaching a bandwidth of 1.67 GHz.

The enhancement occurs because the FSS introduces a controlled electromagnetic environment above the antenna surface, influencing surface current paths and creating additional resonant modes. The use of a dielectric layer like FR-4 (with $\varepsilon_r = 4.4$) between the patch and FSS further supports resonance shifting and confinement. This leads to better field confinement and improved coupling to nearby materials—making the FSS-loaded antenna more suitable for sensing applications.

Thus, this study reinforces the potential of FSS-integrated antennas not only in radiation and stealth applications but also in near-field sensitive material detection. The learnings from this work were foundational in motivating the use of **custom-shaped FSS units** in the present thesis for sensor enhancement.

2.5 Hexagonal Unit Cells for Miniaturized and High-Sensitivity Design

While the use of square-shaped FSS elements and cross-fractal geometries in literature shows measurable benefits, the current thesis adopts **hexagonal unit cells** for several reasons. Firstly, **hexagonal shapes offer superior space-filling efficiency** compared to square or circular resonators. Their six-fold symmetry allows for tighter packing and better angular uniformity, which is beneficial for both isotropic radiation and local field distribution.

Secondly, hexagonal geometries exhibit **more uniform surface current distribution** and **improved resonant behavior** due to their compact perimeter-to-area ratio. This leads to increased interaction between the antenna's evanescent near-field and materials placed near its surface, thereby enhancing sensitivity. Unlike standard FSS implementations that target RCS reduction or multi-band filtering, the hexagonal cells in this work are embedded strategically around the patch to **localize and intensify the near-field response** for sensing purposes.

Additionally, HFSS simulation results show that antennas with hexagonal unit cells demonstrate better miniaturization while maintaining high sensitivity. The design successfully detects small-sized materials (as small as $5 \times 5 \times 2$ mm) placed at a

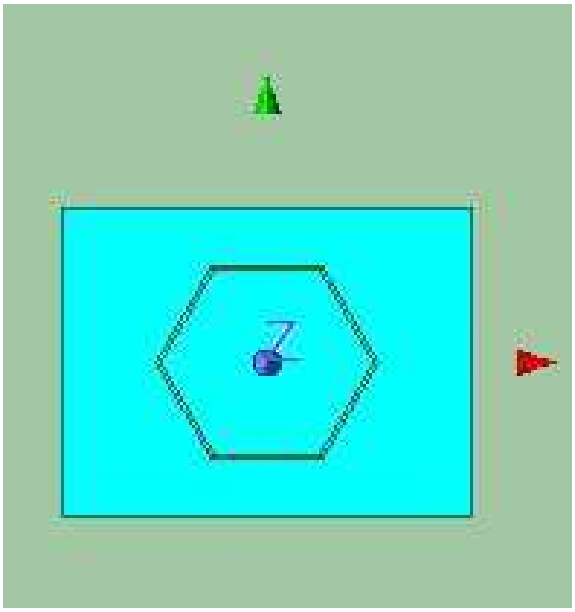

FIGURE 2.2: Hexagon unit cell

2 mm distance from the patch, with noticeable shifts in S_{11} and resonant frequency, validating its suitability for high-resolution sensing applications.

In summary, the adoption of hexagonal FSS-inspired elements in this thesis is a deliberate design evolution that balances the benefits of metamaterial effects with practical constraints like compactness, manufacturability, and sensitivity—key criteria for next-generation antenna-based sensors.

2.6 Hexagonal Unit Cells in Antenna Design

In the paper by [5], while initially aimed at stealth applications, offers valuable insights into the use of metamaterial-inspired Frequency Selective Surface (FSS) structures in antenna miniaturization. The authors introduce hexagonal-shaped FSS unit cells on a dielectric substrate ($\varepsilon_r = 2.55$, thickness = 0.8 mm) to surround a rectangular slot antenna resonating at 3.4 GHz.

The hexagonal FSS behaves as a band-stop filter that alters the surface current paths, reducing radar visibility in out-of-band frequencies while preserving in-band radiation characteristics. More importantly for this thesis, these unit cells exhibit metamaterial properties that modify local permittivity and permeability, improving near-field confinement and surface wave control—traits essential for material sensing.

Though designed for radar signature suppression, this structure inspired the integration of hexagonal metamaterial cells in the current work. Unlike the square SSRRs used in earlier studies, hexagonal cells offer greater spatial compactness and symmetry, enabling better near-field enhancement around the patch. HFSS simulations confirmed that embedding hexagonal cells improves sensitivity to nearby materials and allows for frequency shifts that correlate with dielectric variations.

This paper demonstrates that FSS-based metamaterial structures, though traditionally used in RCS manipulation, have strong potential in sensing applications when re-engineered for enhanced electromagnetic interaction. The present work adapts this concept to design a sensitive, miniaturized patch antenna capable of detecting small-scale materials placed close to the antenna surface.

Chapter 3

Study Methodology

3.1 Overview

The core objective of this study is to design and analyze a metamaterial-integrated microstrip patch antenna with high sensitivity to detect variations in the properties of materials placed near it. This chapter outlines the methodology adopted to achieve that goal—beginning with the simulation strategy, evaluation parameters, tool environment, and the systematic steps followed in developing and testing various antenna configurations.

3.2 Simulation Environment

All antenna structures were modeled and simulated using **Ansys HFSS**, a leading 3D full-wave electromagnetic simulation tool based on the Finite Element Method (FEM). HFSS offers precise control over boundary conditions, adaptive meshing,

and advanced field calculations, making it ideal for high-frequency applications like antenna design and material characterization.

The key simulation setup included:

- **Frequency range:** 5 to 25 GHz
- **Excitation:** Modal Wave port(s)
- **Boundary condition:** Radiation boundary
- **Substrate:** FR-4 ($\varepsilon_r = 4.4$), thickness 0.8 mm (unless otherwise noted)
- **Evaluation:** S_{11} and S_{22} parameters, bandwidth, and resonance shift

3.3 Simulation Workflow

The simulation methodology followed a stepwise progression:

3.3.1 Step 1: Replication of Base Design from Literature

As a foundational step, the microstrip patch antenna from [1] work on metamaterial sensors was replicated. This involved designing a rectangular patch antenna at the desired operating frequency (around 12 GHz) and analyzing its baseline S-parameter performance without any metamaterial structures.

3.3.2 Step 2: Incremental Addition of SRRs

Once the base antenna's performance was validated, square split ring resonators (SSRRs) were added sequentially. After each inclusion, the reflection coefficient (S_{11})

was measured to understand how each SRR influenced the resonance and impedance matching. This stage was critical in assessing the role of individual metamaterial elements in enhancing the sensing potential of the antenna.

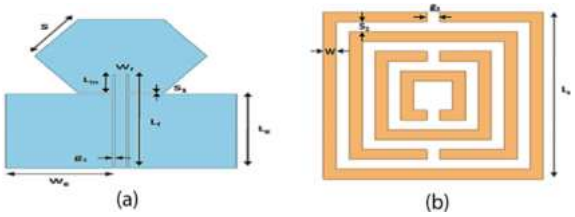

FIGURE 3.1: Reference image for multiple SRR added

3.3.3 Step 3: Material Placement and Sensitivity Testing

With the SRR-enhanced antenna, material samples were modeled and placed in proximity to the radiating surface. Initially, the material sample was of similar size to the patch and placed close to the antenna. Variations were tested in:

- Material type (dielectric constant ε_r)
- Thickness of the material
- Distance between material and antenna surface

This phase established the antenna's ability to detect material presence through observable changes in S_{11} and resonant frequency.

3.3.4 Step 4: Motivation for Enhanced Sensitivity with Smaller Samples

Although results showed sensitivity to larger samples, the goal was to detect **much smaller materials** (on the order of millimeters). This led to the next design

phase: adopting additional metamaterial structures—specifically Frequency Selective Surfaces (FSS)—to enhance field confinement and improve sensitivity.

3.3.5 Step 5: Two-Port and Hybrid Antenna Configurations

Two new antennas were designed:

- An antenna with FSS structures and two ports, inspired by [5]
- A hybrid antenna combining both SRRs and FSS elements, also designed with two ports

These designs were simulated under similar material perturbation scenarios as earlier. The two-port setup enabled observation of both reflection and transmission behavior (S_{11} and S_{22}), which provided deeper insight into the sensing dynamics.

3.4 Sensitivity Evaluation Criteria

To evaluate material sensitivity, the following simulation outputs were monitored:

- Shift in resonant frequency due to material placement
- Change in return loss at both ports (S_{11}), (S_{22}) and bandwidth
- Change in transmission coefficient (S_{21}) for two-port designs and checking if there is any interaction between the ports and thrive for isolation between the ports

The detection of smaller materials was quantified by the magnitude of S-parameter variation in response to changes in material properties.

3.5 Validation through Fabrication

To verify the correctness of simulated resonance behavior, one of the SRR-based antenna designs was fabricated using a PCB process. Vector Network Analyzer (VNA) measurements were conducted to ensure that the fabricated antenna matched the simulated resonant frequency. This confirmed the design's viability for real-world implementation, although experimental material testing was beyond the scope of this phase.

3.6 Summary

This chapter outlined the end-to-end simulation methodology used in the study—from literature-based replication to iterative optimization using metamaterial inclusions and FSS structures. The sensitivity analysis formed the core of this research, guiding the antenna design toward detecting increasingly smaller materials with measurable electromagnetic response.

Chapter 4

Antenna Design and Variations

4.1 Introduction

This chapter presents the different antenna structures developed over the course of this work. Starting from a standard microstrip patch antenna, progressive enhancements were made by incorporating split ring resonators (SRRs), Frequency Selective Surface (FSS) structures, and hybrid combinations of both. Each design is discussed with reference to its geometry, design rationale, and simulation results. Tables and figures included in this chapter document the dimensional parameters and their effect on antenna performance.

4.2 Base Patch Antenna Design

The initial antenna design consisted of a rectangular patch resonating in the X-band, with FR-4 as the substrate. This design served as the baseline for observing how

metamaterial elements could modify the response. The S_{11} plot showed a single dominant resonance with modest return loss and bandwidth.

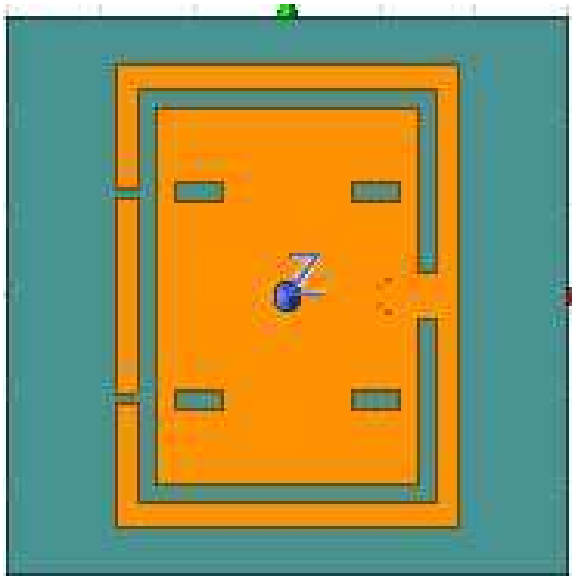

FIGURE 4.1: Base antenna with one SRR

4.3 SRR-Loaded Patch Antenna

The design from [1] was replicated, starting with no SRRs and gradually adding square SRRs one by one. The geometry of each SRR was carefully chosen to ensure it would induce resonance near the operating frequency.

Key observations to be noted:

- Each SRR addition caused a small downward shift in resonant frequency
- Return loss improvement for various steps
- Coupling increased in near-field zones

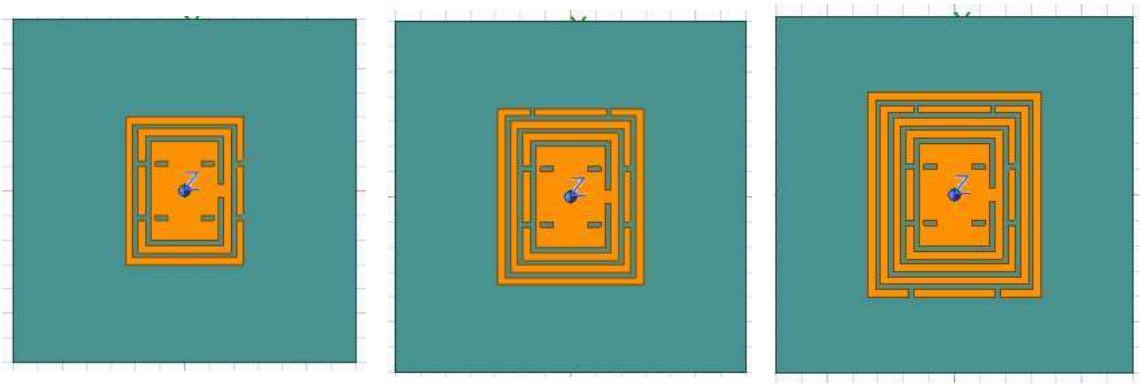

(a) Two SRRs (b) Three SRRs (c) Four SRRs

FIGURE 4.2: Each step in the design of the antenna

4.4 Material Sensitivity Simulation with SRRs

With the SRR-enhanced design, large-sized materials (same footprint as the patch) were placed near the antenna at varying distances and dielectric values. The goal was to establish a performance benchmark for known materials. The following findings were to be noted

- S_{11} shifted significantly for high-ε_r materials
- Variation with thicker materials caused deeper notches in reflection
- Farther placement of the material and noticing the sensitivity

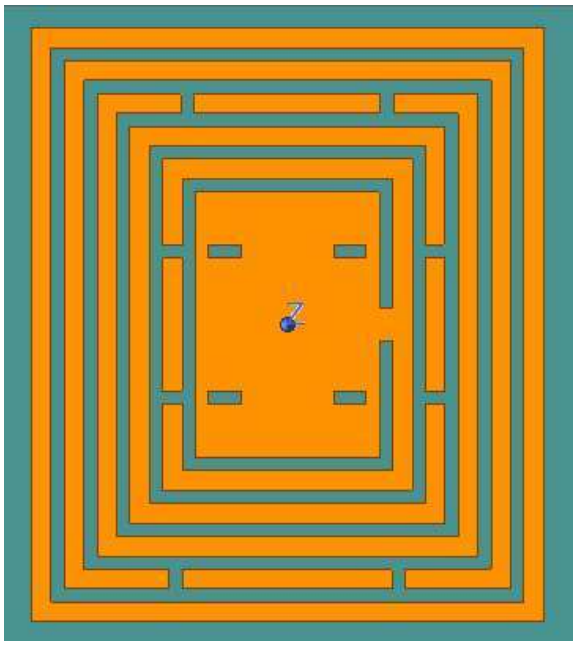

FIGURE 4.3: Complete antenna design with SRRs

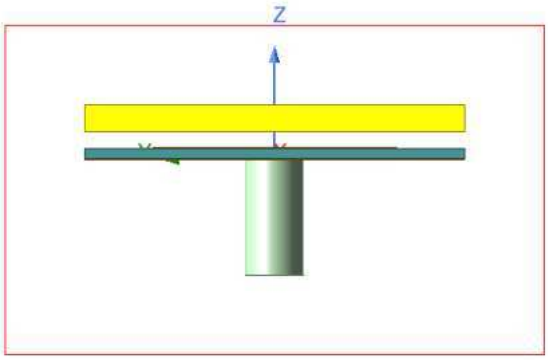

FIGURE 4.4: Material placed near the antenna

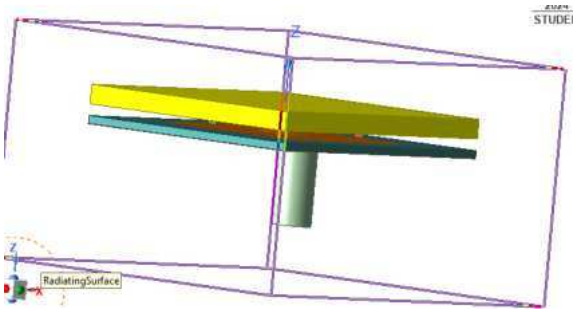

FIGURE 4.5: Orthogonal view of material placed

TABLE 4.1: Full SRR Antenna Parameters

Name	**Value**	**Description**
pt	2.17	Feed point value or excitation location
sub_x	28mm	Width of the substrate
sub_y	28mm	Height of the substrate
sub_t	0.8mm	Substrate thickness
m1	5.6mm	Dimension of first SRR element
m1_y	8.103mm	Y-position of first SRR element
m1_x	5.6mm	X-position of first SRR element
thi	0.035mm	Thickness of metal layer
inn_r	0.45mm	Inner radius of the SRR
out_r	(4.26/2) mm	Outer radius of the SRR
cutx	1mm	X-direction cut length in SRR ring
cuty	0.4mm	Y-direction cut width in SRR ring
f	1.5	Operating frequency factor or coefficient
out_r_in	2.03mm	Inner outer ring distance
gnd_x	28mm	Ground plane width
gnd_y	28mm	Ground plane height
sc_h	8.5mm	Substrate cavity height or port height
m2_x	7.4mm	X-position of 2nd SRR ring
m2_y	10mm	Y-position of 2nd SRR ring
gap1	0.4mm	Gap between 1st and 2nd SRR
con_st2_st3	1mm	Connector/stub dimension between stage 2 and 3
sl_w	0.4mm	Slot width
m3_x	m2_x+2*srr_diff	X-position of 3rd SRR, based on spacing
m3_y	m2_y+2*srr_diff	Y-position of 3rd SRR
gap2	0.4mm	Gap between 2nd and 3rd SRR
m4_x	m3_x+2*srr_diff	X-position of 4th SRR
m4_y	m3_y+2*srr_diff	Y-position of 4th SRR
gap3	0.4mm	Gap between 3rd and 4th SRR
m5_x	m4_x+2*srr_diff	X-position of 5th SRR
m5_y	m4_y+2*srr_diff	Y-position of 5th SRR
gap4	0.4mm	Gap between 4th and 5th SRR
m6_x	m5_x+2*srr_diff	X-position of 6th SRR
m6_y	m5_y+2*srr_diff	Y-position of 6th SRR
gap5	0.4mm	Gap between 5th and 6th SRR
mat_t	2mm	Thickness of material placed near antenna
dis	2mm	Distance of material from antenna
mat_x	sub_x+0mm	Material X-position
mat_y	sub_y+0mm	Material Y-position
srr_diff	1mm	Differential spacing between SRRs

4.5 Design with FSS-Based Metamaterials

Inspired by [5], a new design incorporating **hexagonal FSS cells** was developed. This antenna was made with two ports to observe both transmission and reflection.

Design notes:

- The hexagonal geometry offered tighter packing and angular symmetry
- Enhanced local field confinement was noted
- Higher sensitivity to smaller samples compared to earlier designs

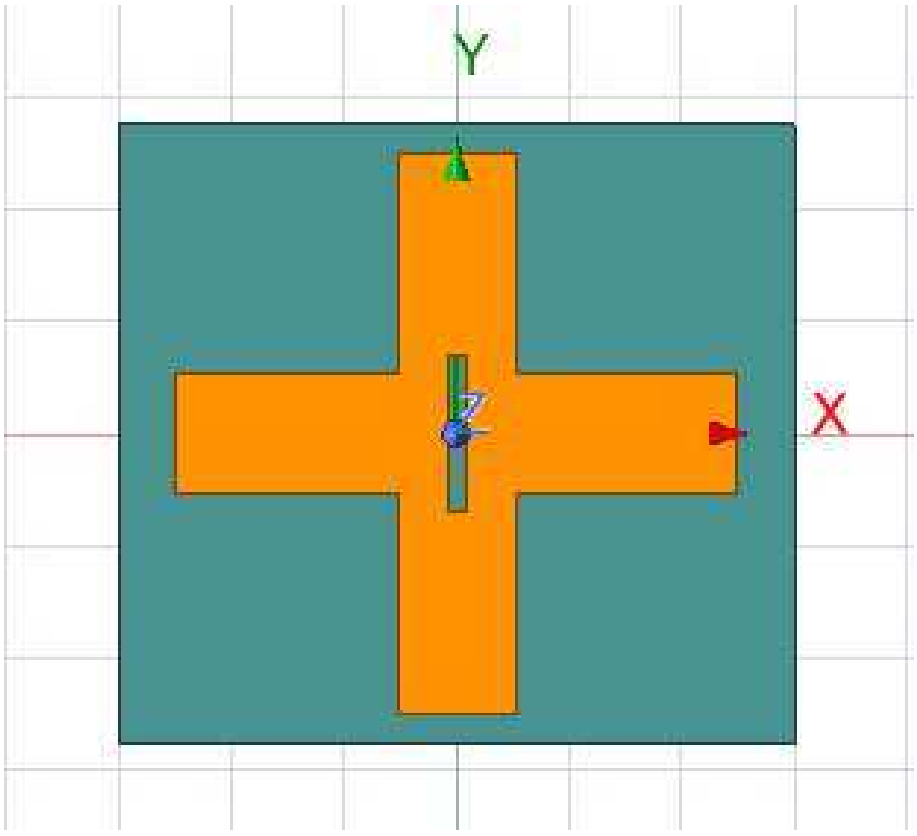

FIGURE 4.6: Slab antenna without hexagonal unit cells

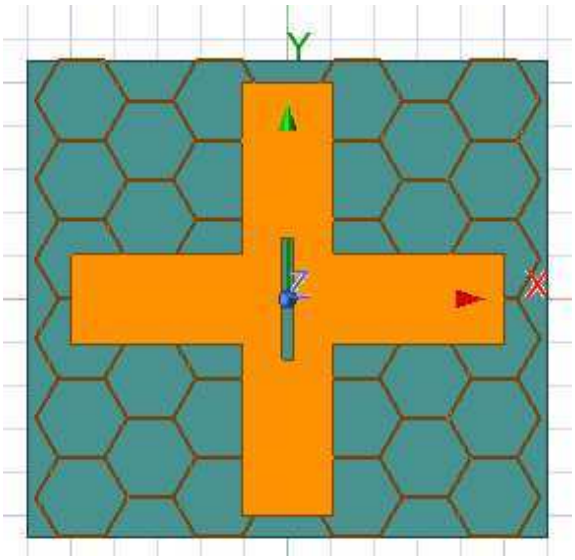

FIGURE 4.7: Antenna with hexagonal cells added

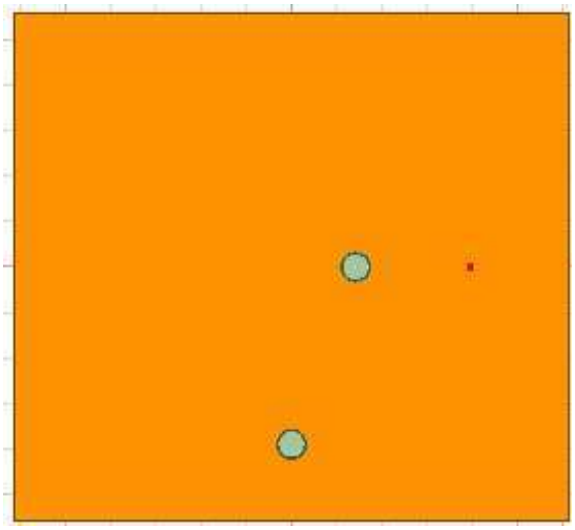

FIGURE 4.8: Port view for slab antenna

4.6 Hybrid SRR + FSS Antenna

A novel antenna combining both SRRs and hexagonal FSS units was designed. The goal was to merge the localized resonance of SRRs with the broad filtering capability of FSS. This antenna also employed a two-port structure.

After designing the antenna, a material of relatively smaller size(5 mm x 5 mm x 2

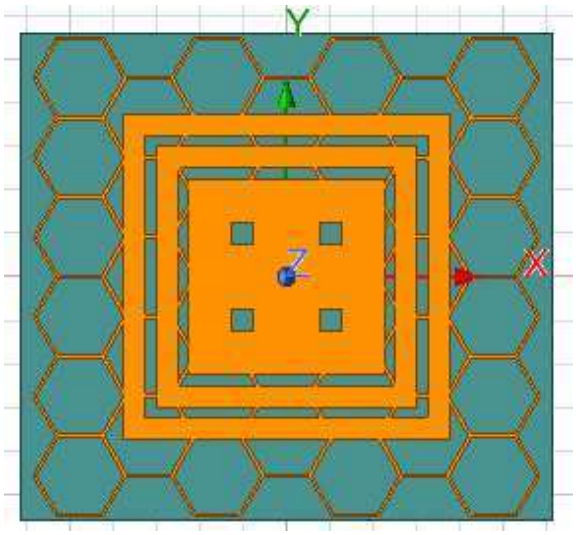

FIGURE 4.9: SRR antenna combined with hexagonal unit cells

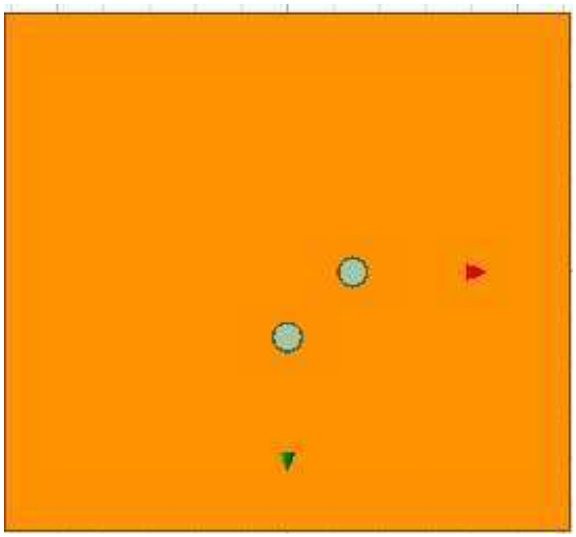

FIGURE 4.10: Port view for antenna with SRR integrated with hexagonal cells

mm) is kept near the antenna, and the variation in S-parameters and field variations are noted

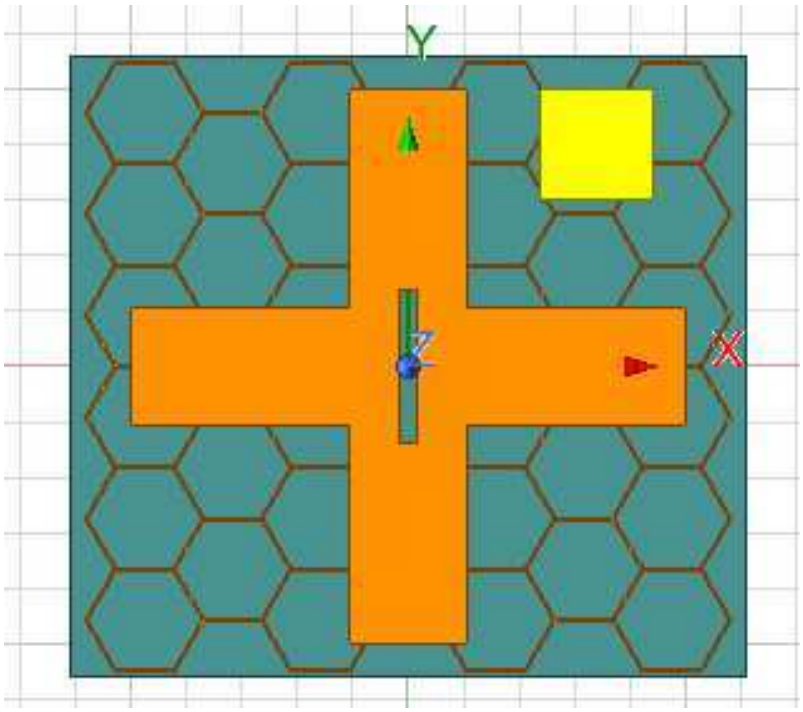

FIGURE 4.11: Object placed between the two ports

4.7 Fabrication and Measurement

Both the FSS-based antennas were fabricated on an FR-4 board and measured using a VNA for S-parameter analysis. Results closely matched simulated resonant frequencies, validating the HFSS-based design approach. The following tables give the design parameters for both the fabricated antennas

TABLE 4.2: FSS Slab Antenna Parameters

Name	**Value**	**Description**
unit_x	40mm	Unit cell width
unit_y	30mm	Unit cell height
unit_t	0.035mm	Conductor thickness
hex_s	10.8mm	Hexagonal structure size
hex_out	10.8mm	Outer dimension of hexagon
hex_diff	0.4/(sqrt(3)) mm	Distance between hexagon and its inner layer
hex_in	hex_out - 2*hex_diff	Inner dimension of hexagon
rec_x	122mm	Rectangle width
rect_y	112mm	Rectangle height
sub_rec_diff	0mm	Substrate margin from rectangle
sub_x	rect_x + 2*sub_rec_diff	Substrate width
sub_y	rect_y + 2*sub_rec_diff	Substrate height
sub_t	1.6mm	Substrate thickness
gnd_rec_diff	0.5mm	Ground margin difference
gnd_x	rect_x	Ground width
gnd_y	rect_y	Ground height
rect_x	rec_x	Mapped rectangle width
rec_y	rect_y	Mapped rectangle height
inn_r	0.9mm	Inner radius for circular features
out_r_in	3mm	Outer ring inner radius
m1_x	30mm	X-position of main patch
thi	0.035mm	Metal layer thickness

sc_h	8.5mm	Substrate cavity height or port height
out_r	3.2mm	Outer radius
strip_back_y	2.2mm	Y-length of strip behind patch
strip_back_x	2.5mm	X-length of strip behind patch
via_r	strip_back_y	Via radius
slab_x	21mm	Slab width
slab_y	100mm	Slab height
cutslot_x	3mm	Slot width for cuts
cutslot_y	28mm	Slot height for cuts
m2_x	80mm	X-location of second patch or slab
obj_x	obj_y	X-dimension of object near slab
obj_y	10mm	Y-dimension of object
obj_z	2mm	Z-dimension of object
dist	5mm	Distance of object from slab
obpos_x	0	Object X-position
obpos_y	m2_x/2 - inn_r	Object Y-position
obpos_z	5mm	Object Z-position
er_material	1	Relative permittivity of material
tand_material	0.005	Loss tangent of material

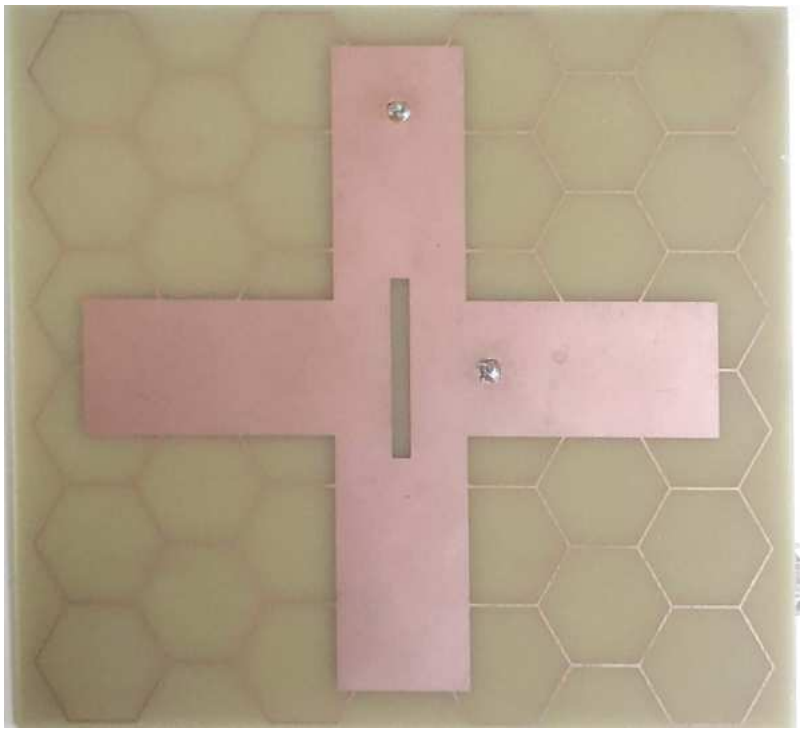

FIGURE 4.12: Fabricated FSS Patch Antenna

TABLE 4.3: SRR+FSS Antenna Parameters

Name	**Value**	**Description**
unit_x	40mm	Unit cell width
unit_y	30mm	Unit cell height
unit_t	0.035mm	Conductor thickness
hex_s	10.8mm	Hexagonal structure size
hex_out	10.8mm	Outer dimension of hexagon
hex_diff	0.35mm	Hexagonal ring thickness or gap
hex_in	hex_out - 2*hex_diff	Inner dimension of hexagon
rec_x	122mm	Rectangle width
rect_y	112mm	Rectangle height
sub_rec_diff	0mm	Substrate margin from rectangle
sub_x	rect_x + 2*sub_rec_diff	Substrate width

sub_y	rect_y + 2*sub_rec_diff	Substrate height
sub_t	0.8mm	Substrate thickness
gnd_rec_diff	0mm	Ground margin difference
gnd_x	rect_x + 2*gnd_rec_diff	Ground plane width
gnd_y	rect_y + 2*gnd_rec_diff	Ground plane height
rect_x	rec_x	Mapped rectangle width
rec_y	rect_y	Mapped rectangle height
inn_r	0.9mm	Inner radius for circular features
out_r_in	3mm	Outer ring inner radius
m1_x	30mm	X-position of primary patch
thi	0.035mm	Metal layer thickness
sc_h	8.5mm	Substrate cavity height or port height
out_r	3.2mm	Outer radius
strip_back_y	2.2mm	Y-dimension of strip behind patch
strip_back_x	2.5mm	X-dimension of strip behind patch
via_r	strip_back_y / 2	Via radius
slab_x	100mm	Slab width
slab_y	100mm	Slab height
cutslot_x	3mm	Slot width for cutting
cutslot_y	28mm	Slot height for cutting
slab2_x	75mm	Second slab width
slab2_y	75mm	Second slab height

slab1_x	80mm	First slab width
slab1_y	80mm	First slab height
slab3_x	65mm	Third slab width
slab3_y	65mm	Third slab height
slab4_x	60mm	Fourth slab width
slab4_y	60mm	Fourth slab height
slab5_x	50mm	Fifth slab width
slab5_y	50mm	Fifth slab height
slab6_x	55mm	Sixth slab width
slab6_y	55mm	Sixth slab height
slitwidth	5mm	Slit width
slitx	10mm	X-dimension of slit
slity	10mm	Y-dimension of slit
slitwidthx	5mm	Alternate slit width
slitlength	5mm	Slit length
m2_x	30mm	X-position of secondary patch
obpos_x	m1_x / 2 - inn_r	Object X-position
obj_x	10mm	Object X-dimension
obpos_y	0mm	Object Y-position
obj_y	10mm	Object Y-dimension
obpos_z	5mm	Object Z-position
obj_z	5mm	Object Z-dimension
er_material	1	Relative permittivity of material
tand_material	0.031	Loss tangent of material

FIGURE 4.13: Fabricated SRR+FSS Patch Antenna

4.8 Summary

This chapter documents the design evolution of the antenna—from a basic patch to complex metamaterial-enhanced structures—and highlights the performance gains achieved. The final antenna, featuring hexagonal FSS units and SRRs, offered the best trade-off between size and sensitivity, making it suitable for compact material sensing applications.

Chapter 5

Analysis and Results

5.1 Introduction

This chapter presents the analysis of simulation results obtained from various antenna configurations designed in the previous chapter. The primary objective is to evaluate the performance of each design in terms of its sensitivity to materials placed in close proximity, with a focus on observing variations in key electromagnetic parameters such as return loss (S_{11}), resonant frequency, bandwidth

Each antenna was simulated using Ansys HFSS under controlled conditions, and its response was recorded with and without material presence. Starting from a baseline patch antenna, successive improvements were made by incorporating split ring resonators (SRRs), Frequency Selective Surface (FSS) elements, and ultimately a hybrid configuration that combines both techniques. The progression in design was aimed at enhancing the antenna's ability to detect subtle changes in material

properties—particularly for small-sized samples—through measurable shifts in its scattering parameters.

This chapter systematically discusses:

- The electromagnetic performance of each antenna variation
- The effect of introducing materials of different permittivities, thicknesses, and distances from the patch
- A comparative analysis of all designs with respect to sensitivity and design compactness

The results are visualized through S-parameter plots, field distributions, and performance tables. These analyses validate the role of metamaterial integration in improving sensing characteristics and support the final design choice made in this thesis.

5.2 SRR Antenna results

When the substrate and ground size are increased by 10mm from the initial parameters, keep- ing other parameters unchanged from initial values, there is a slight change in the S11 value, but the resonant frequency is intact and unchanged

We could see that the resonant frequency is nearly **17.1GHz** with S11 value of nearly **-28dB**. With variation in substrate permittivity, the resonant frequency increases and shifts to **18.2GHz** for 1.7 permittivity.

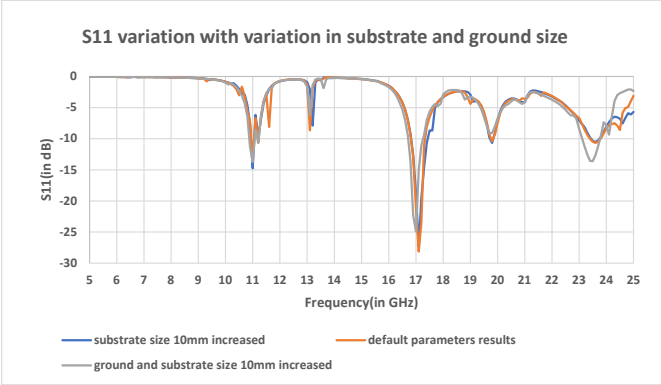

FIGURE 5.1: Variation of S11 with change in substrate and ground size

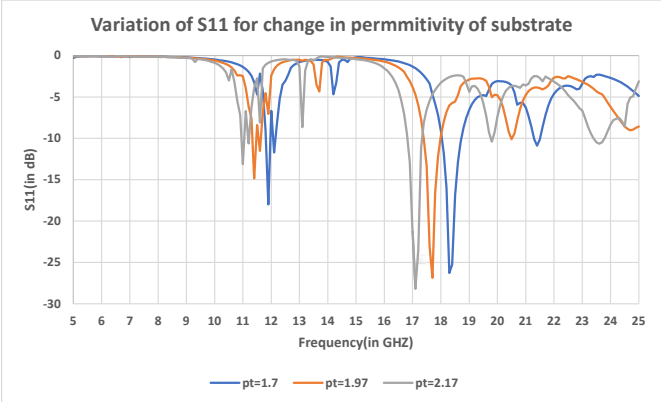

FIGURE 5.2: Variation of S11 with change in permittivity of substrate material

5.2.1 Results for different variations of same material placed

When the distance at which the material is placed is changed, there is a significant change in resonant frequency shift. When the material is placed very near to the antenna(0.8mm), the resonant frequency is shifted to **15.5GHz** and **9.8GHz**, and the values of S11 are increased from the initial values, they are near to **-10dB** when

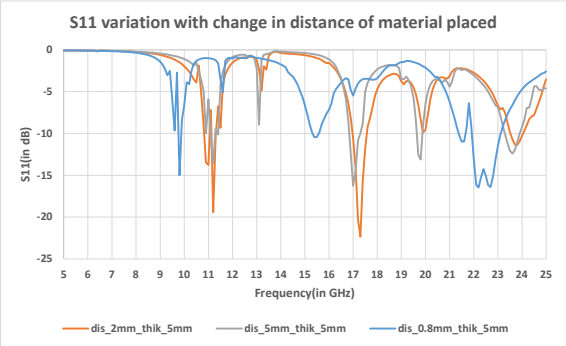

FIGURE 5.3: Variation of S11 with change in the distance at which material is placed

the material is very near to antenna. We could also see that when the distance changed from 5mm to 2mm, the resonant frequency was almost same(17GHz) and there is only a change in the S11 value; it changed from **-23dB** to **-16dB** fig.(5.3)

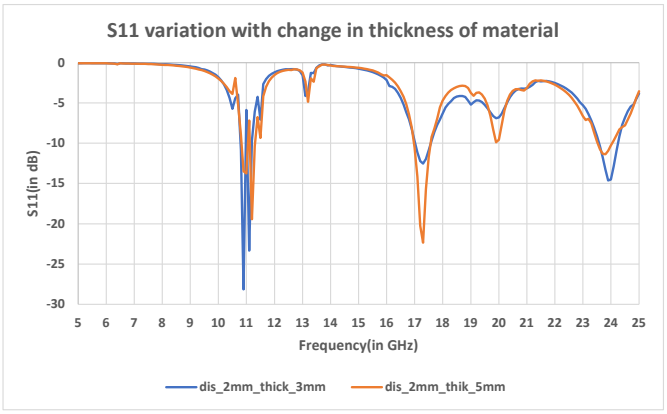

FIGURE 5.4: Variation of S11 with change in thickness of the material placed

We could see from the plots that as the thickness of the material placed(at a distance 2mm from the antenna) is increased, the S11 is increased from **-23dB** to **-12dB** at 17GHz and **-26dB** to **-16dB** at 11.2 GHz we could see that as the material is similar

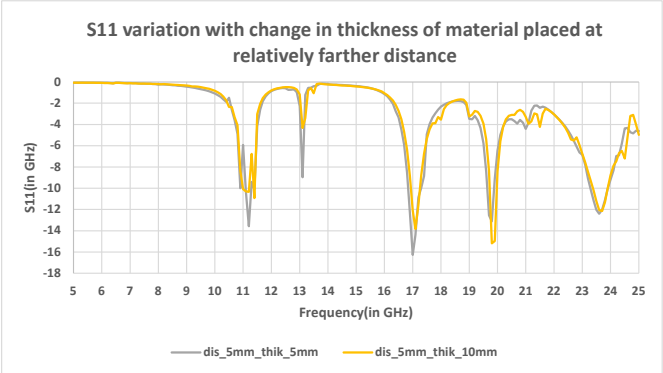

FIGURE 5.5: Variation of S11 with change in thickness of the material placed at a relatively farther distance

to that of the substrate, there is no much change in the resonant frequency, only the S11 value is changed fig.(5.4). Also, we got double resonant frequencies, one at 17 GHz and the other at 11.2 GHz when the material is placed, which shows the variation from the initial condition when there is no material

When the material is kept at a relatively farther distance(5mm), there is not much variation in either S11 resonant frequency even when the material thickness is increased; this shows that the antenna works accurately in the near range of up to 5mm fig.(5.5)

5.2.2 Results for different materials placed

From the above plot fig.5.6, we could see that the S11 and resonant frequency significantly changed when the material placed is a metal. The S11 increased to nearly **-11dB** for all the materials at the initial resonant frequency(17GHz). There is no resonant frequency when a metal is placed near the antenna near 17GHz.

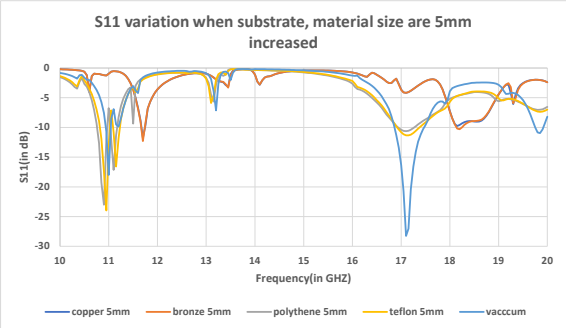

FIGURE 5.6: S11 variation for different materials placed

However, a resonance near 11GHz is almost the same when the material is not placed.

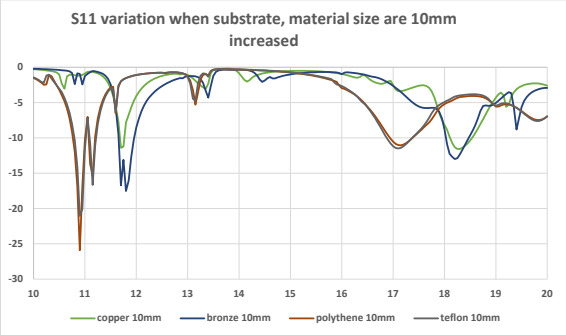

FIGURE 5.7: S11 variation for different material placed

When the material and substrate are 10mm bigger than the initial design size, there is a significant shift in the resonant frequency at 11GHz for the metal material. The resonant frequency is shifted to nearly **11.8GHz** with S11 increased nearly to **-15dB**. Also, there is no resonance at 17GHz

A material of **10mm x 10mm x2mm** is kept at a distance of 2mm from the antenna at position where the E-field is maximum for both the designs from the centre of

the antenna. Now by varying different parameters of the materials, the results of the resonant frequency and S-paramters are tested

Initially, a sample material is created in Ansys HFSS with variable relative permittivity(ϵ_r), conductance(σ), and the S-parameter is observed for variations in these two variables

First, conductance per unit length of the sample material is varied from 1 to 10^6 and the variations in the S-parameters are observed. Later, the relative permittivity of the sample material is varied from 1 to 81, and the variations in the S-parameters are observed. The following section shows the plots of both the observed variations along with the fabricated antenna results

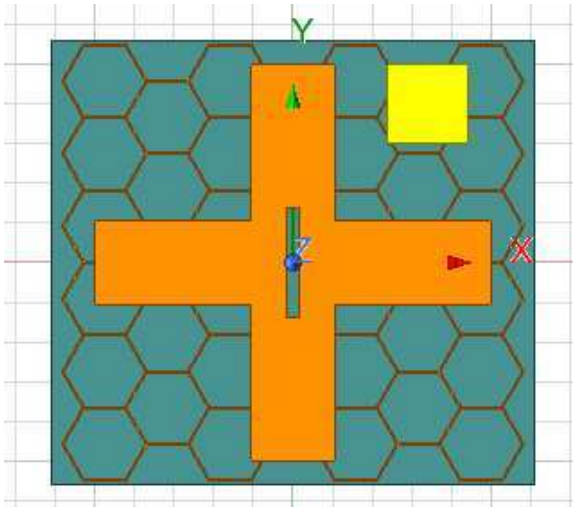

FIGURE 5.8: Sample Position for FSS Antenna

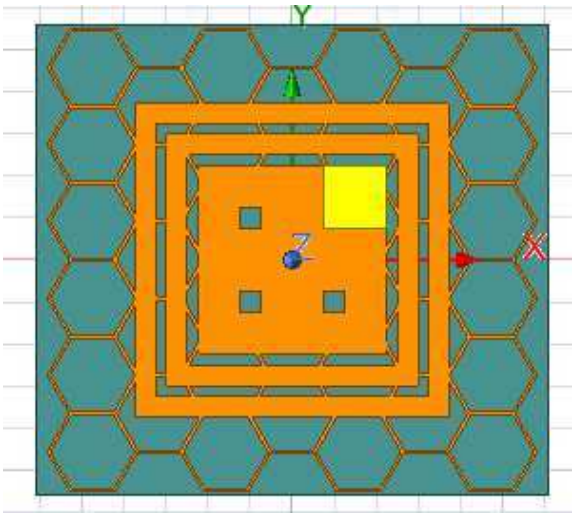

FIGURE 5.9: Sample Position for FSS+SRR Antenna

5.3 FSS Patch Antenna Results

Initially, the antenna is designed and simulated for resonant frequency, later it is fabricated for testing that resonant frequency

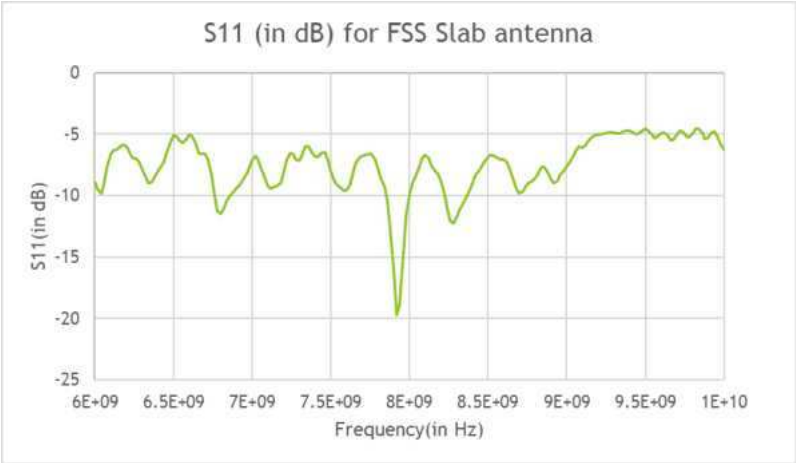

FIGURE 5.10: S11(in dB) for FSS antenna

From the above figures, it could be noted that the resonant frequency for Port 1 is around **7.9GHz** and that of Port 2 is at around **6.9GHz**

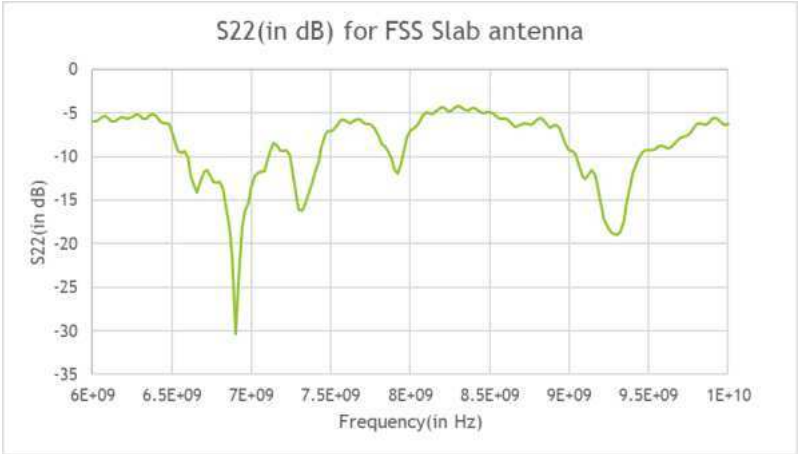

FIGURE 5.11: S22(in dB) for FSS antenna

For checking, there is no interaction between the two ports and are isolated from each other. Parameter S12 is checked, which is the transmission coefficient between the ports. Here, in this case,e S12 is the same as S21

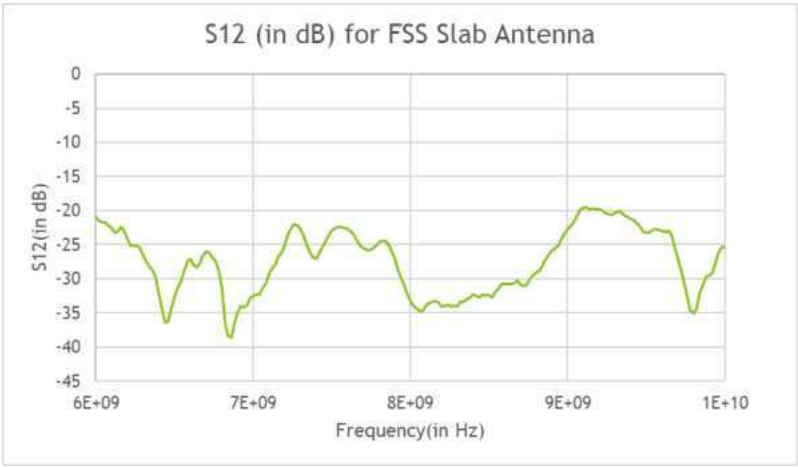

FIGURE 5.12: S12(in dB) for FSS antenna

From the above plot, it can be seen that the S12 value is **less than -20dB** for all the frequencies, which shows that there is no interaction between the ports and they are isolated.

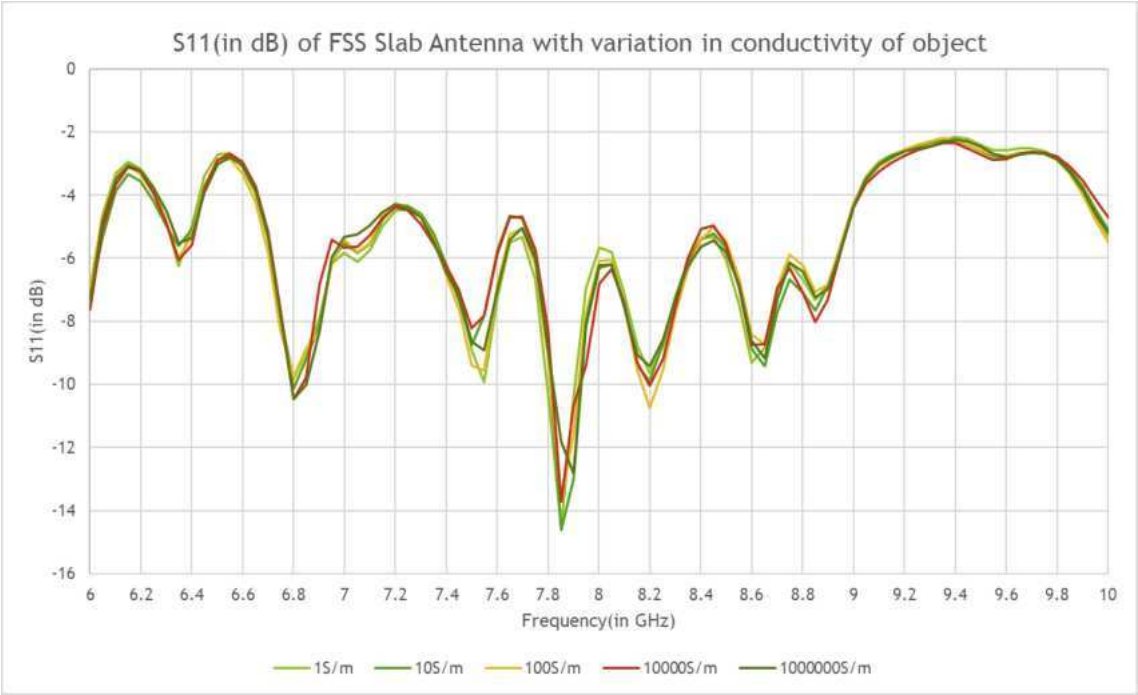

FIGURE 5.13: Variation of S11 with increase in conductance of the material

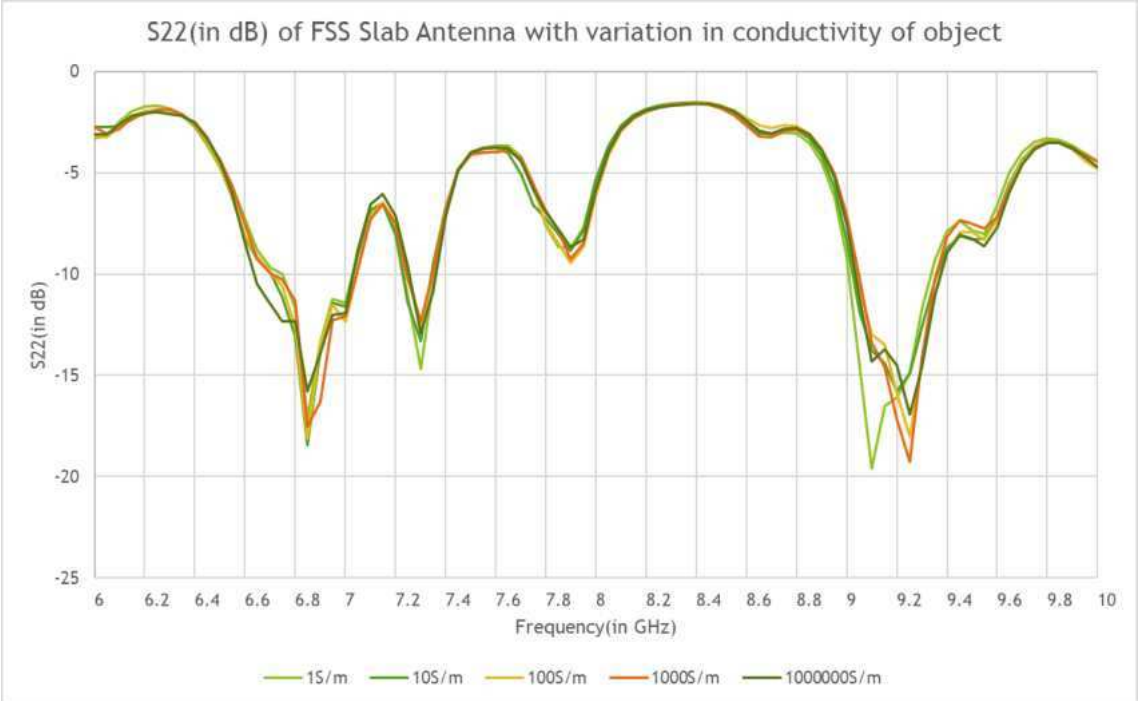

FIGURE 5.14: Variation of S22 with increase in conductance of the material

It is observed from the above graph that as the conductance of the sample material is increased, the value of S11, S22 at the resonant frequency decreases, and also the

3-dB bandwidth at the resonant frequency increases

FIGURE 5.15: Variation of S11 for different materials placed

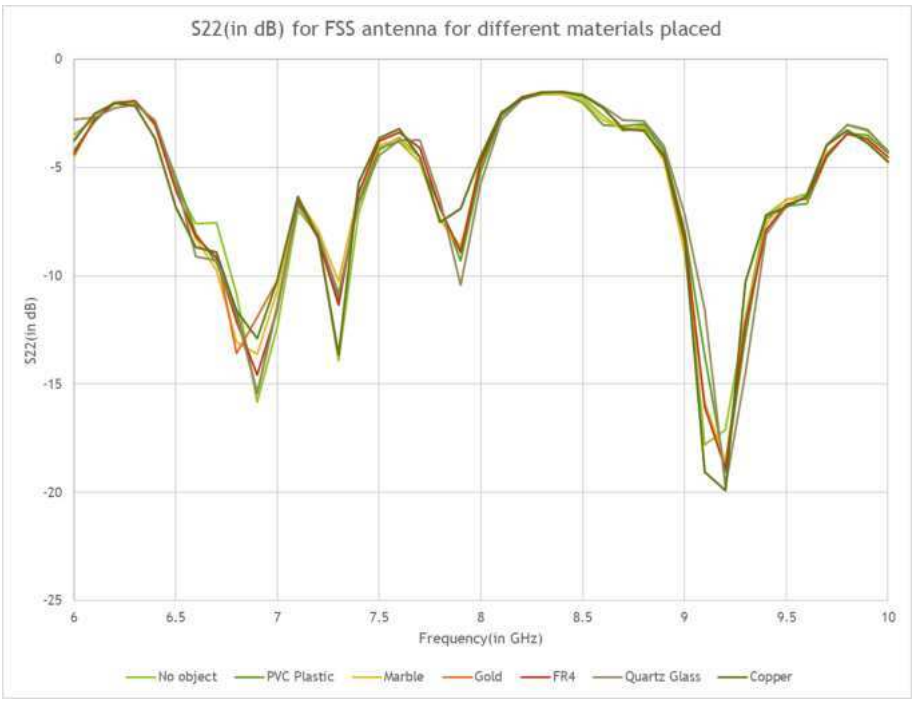

FIGURE 5.16: Variation of S22 for different materials placed

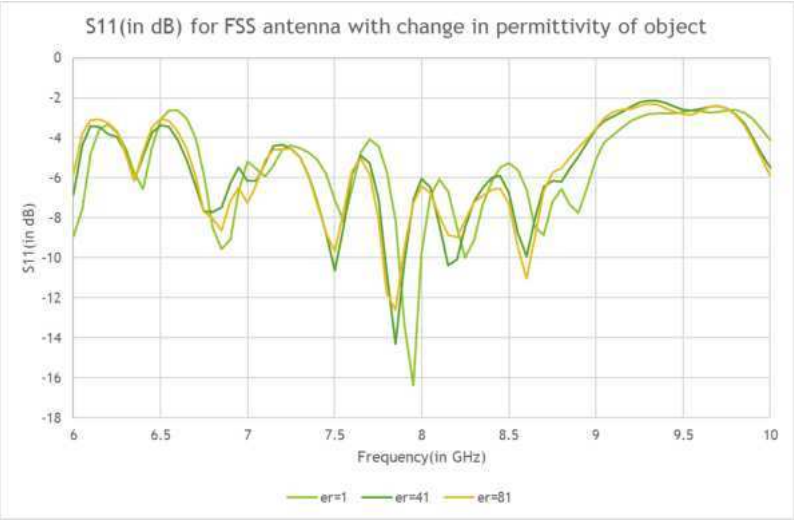

FIGURE 5.17: Variation of S11 with change in relative permittivity(ϵ_r)

5.4 Hybrid FSS+SRR Patch Antenna Results

Initially, the antenna is designed and simulated for resonant frequency, later it is fabricated for testing that resonant frequency

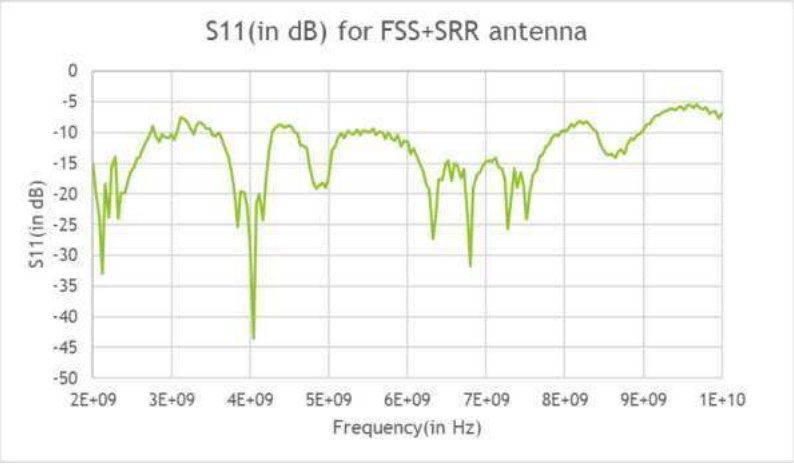

FIGURE 5.18: S11(in dB) for FSS+SRR antenna

From the above figures, it could be noted that the resonant frequency for Port 1 is around **3.95GHz** and that of Port 2 is at around **4.2GHz**

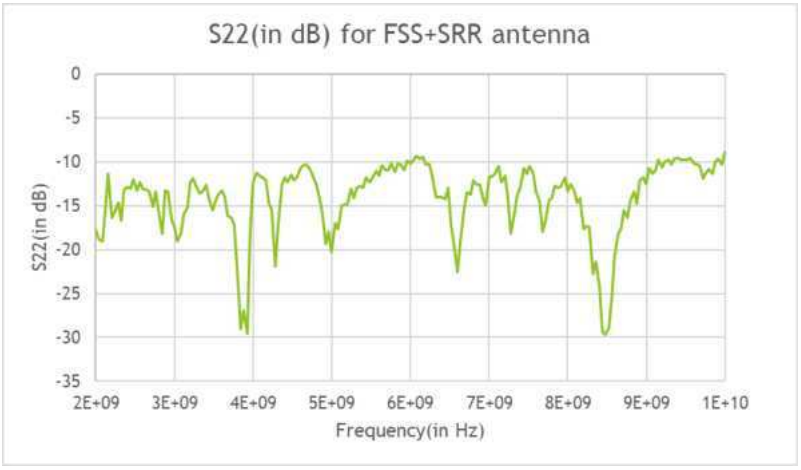

FIGURE 5.19: S22(in dB) for FSS+SRR antenna

For checking, there is no interaction between the two ports and are isolated from each other. Parameter S12 is checked, which is the transmission coefficient between the ports. Here, in this case, S12 is the same as S21. Resonance is considered only when there is no interaction between the ports and both are at isolation(very low S12 value

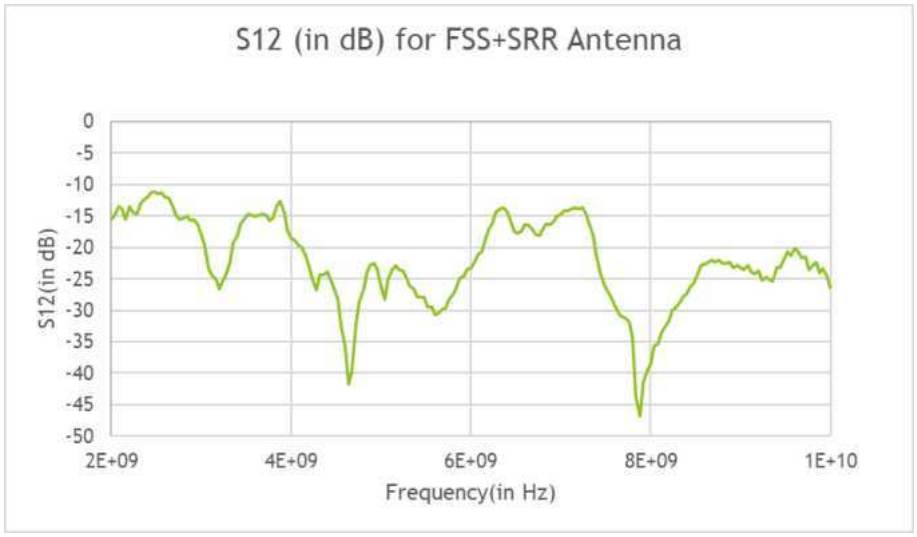

FIGURE 5.20: S12(in dB) for FSS+SRR antenna

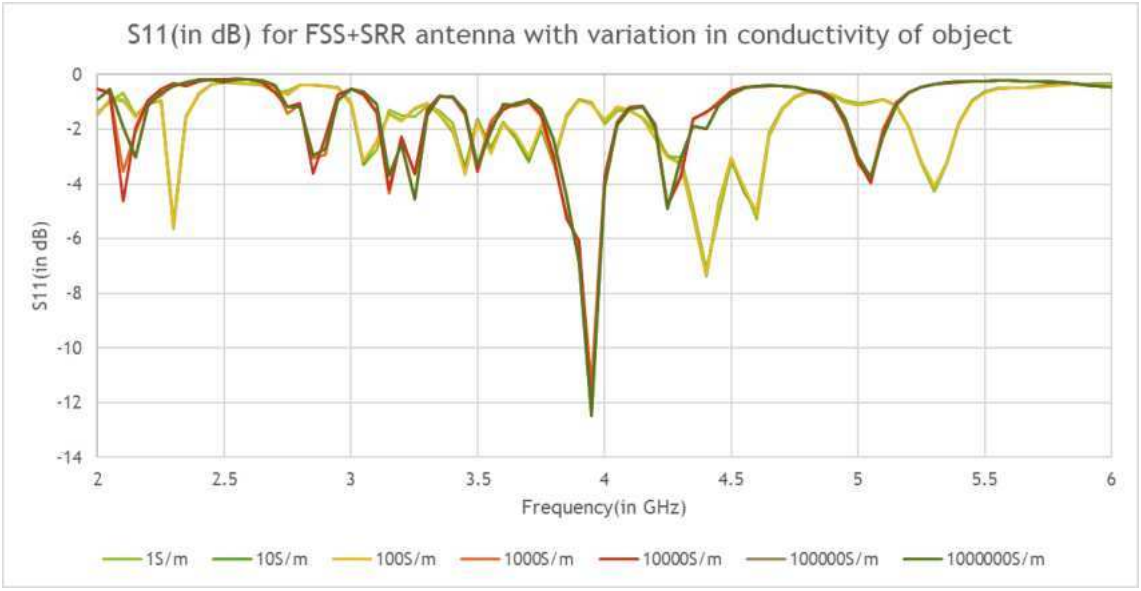

FIGURE 5.21: Variation of S11 with increase in conductance of the material

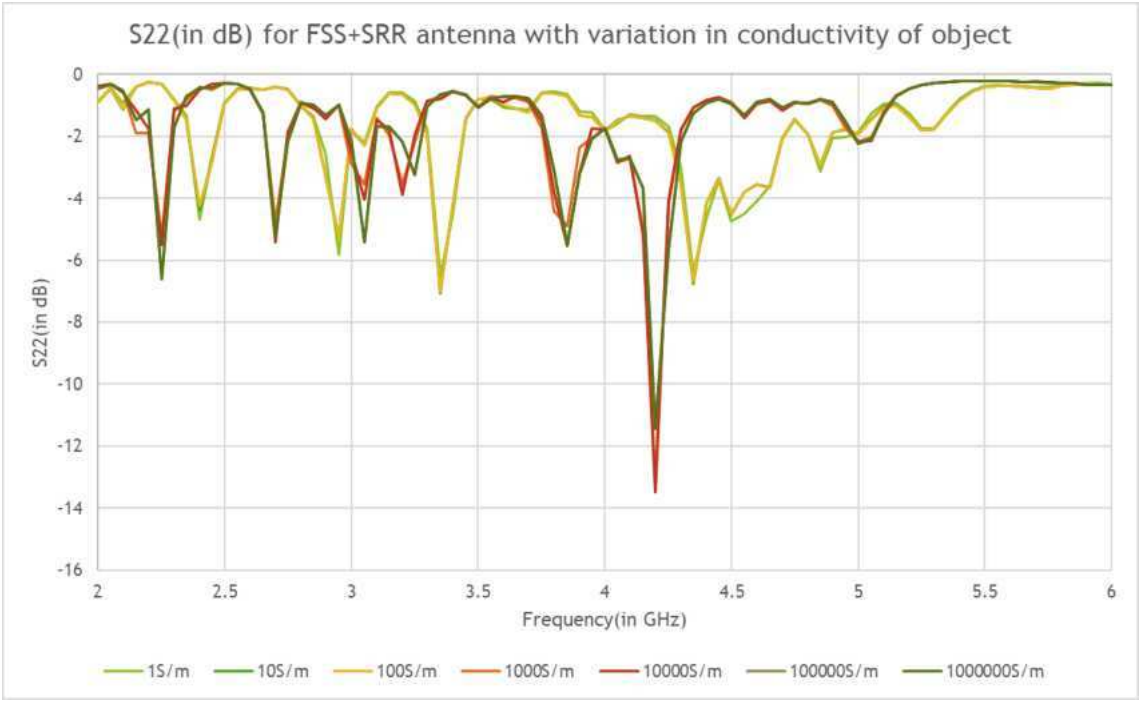

FIGURE 5.22: Variation of S22 with increase in conductance of the material

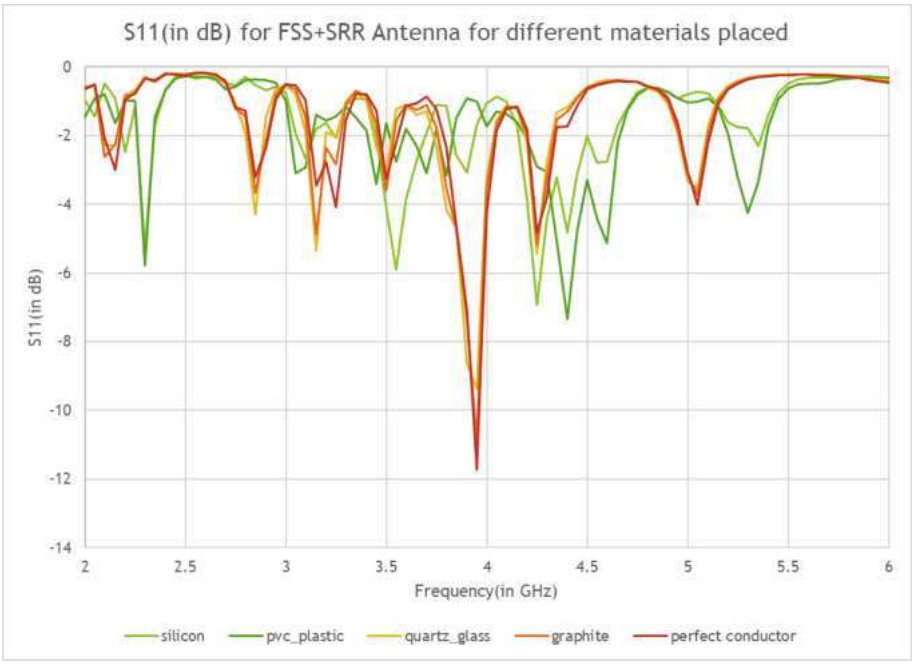

FIGURE 5.23: Variation of S11 for different materials placed

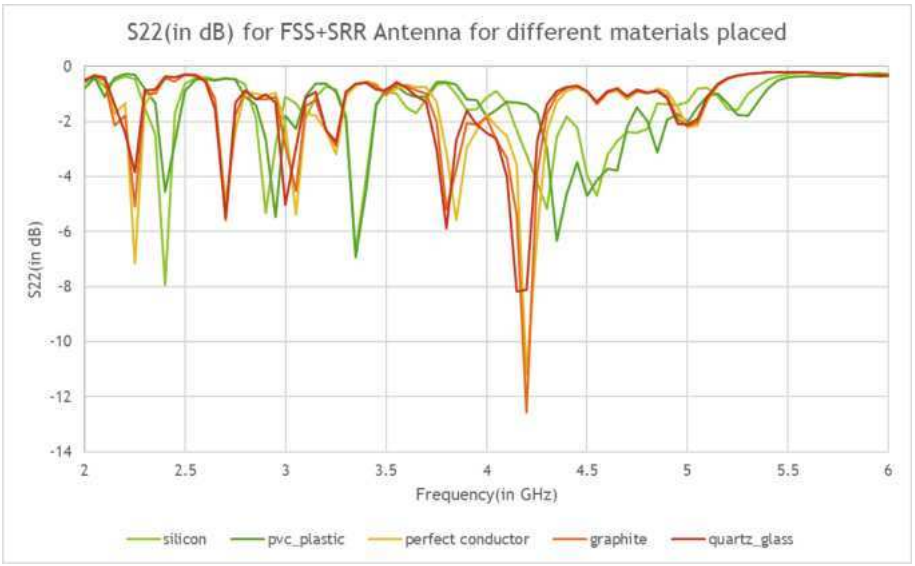

FIGURE 5.24: Variation of S22 for different materials placed

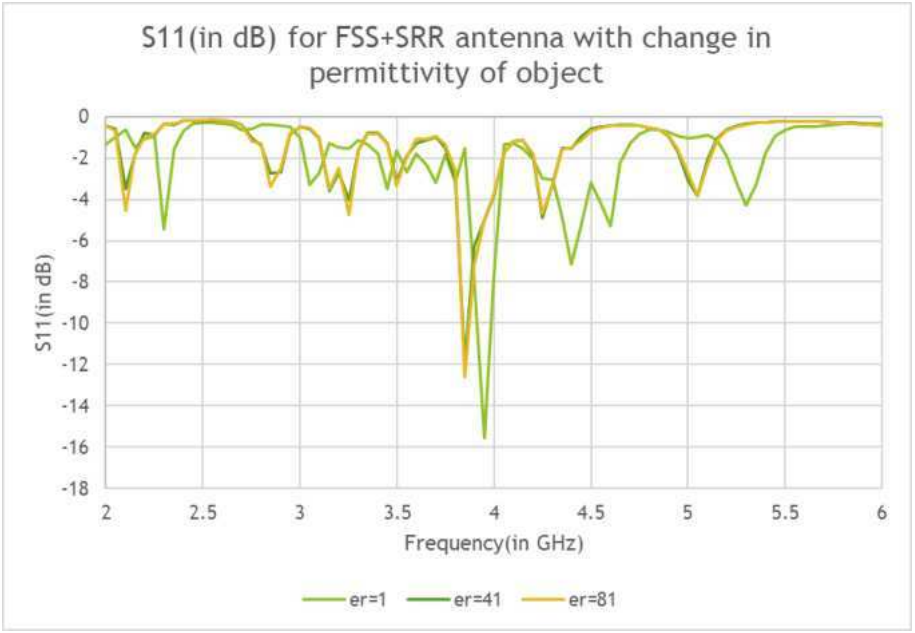

FIGURE 5.25: Variation of S11 with change in relative permittivity(ϵ_r)

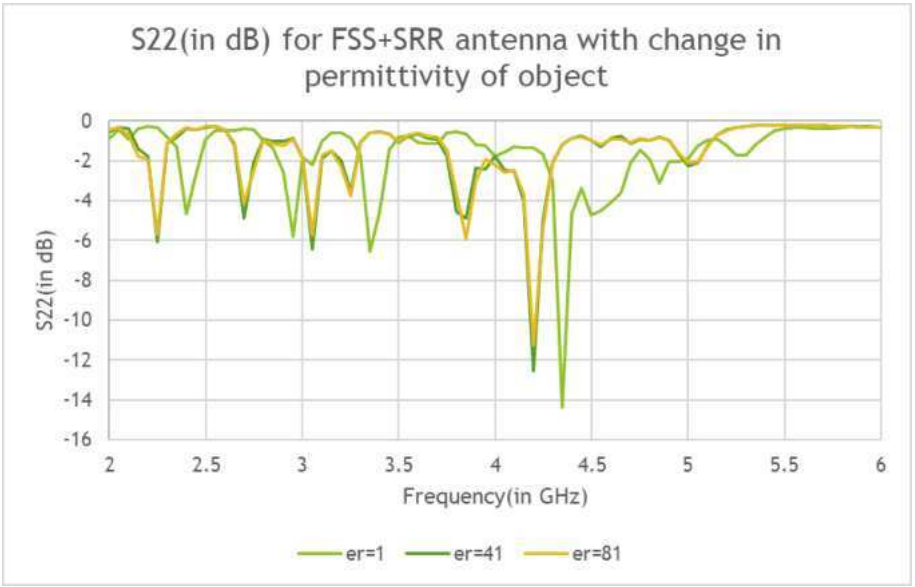

FIGURE 5.26: Variation of S22 with change in relative permittivity(ϵ_r)

Chapter 6

Conclusions and Practical Implications

6.1 FSS Antenna Behavior

The Frequency Selective Surface (FSS)-based antenna, designed using hexagonal unit cells, was tested for its ability to detect and distinguish between different types of materials placed near the patch surface. A small test sample of size $10 \times 10 \times 2$ mm was placed at the electric field hotspot, and its properties (permittivity and conductivity) were varied during simulation.

The following observations were made:

- When a **non-conductive (dielectric)** material was placed, the S-parameters (S_{11}, S_{22}) remained mostly unaffected.

- When a **conductive** material was introduced, the antenna's S-parameters degraded significantly, resulting in a higher reflection coefficient and reduced transmission.
- The antenna was sensitive to conductor proximity but failed to show clear variation for small dielectric perturbations.

These results indicate that while the FSS structure enhances field confinement, it lacks stability in the presence of metallic materials and shows limited effectiveness in distinguishing between material types in complex environments.

6.2 Hybrid FSS + SRR Antenna Behavior

A hybrid antenna integrating both FSS and Split Ring Resonators (SRRs) was designed and tested to improve material detection performance. This antenna retained the advantages of both structures—enhanced field confinement (from FSS) and localized resonance (from SRRs).

The hybrid antenna was tested using the same small material sample setup, and the following behavior was observed:

- When a **conductive** material was placed near the antenna, the S-parameters remained stable and showed minimal deviation.
- When a **non-conductive** or **dielectric** material was introduced, there was a noticeable shift in resonant frequency and return loss.
- The antenna demonstrated high sensitivity and robustness, capable of detecting and differentiating between small dielectric variations.

- Additionally, it was observed that materials with a **high dielectric constant** caused a slight shift in resonant frequency towards lower values.

6.3 Final Conclusions and Classification Method

Based on the simulations and analyses conducted with both antennas, a comparative classification method can be derived from their behavior under various material conditions.

Material Classification Table:

TABLE 6.1: Material classification based on antenna response

Material Category and Characteristics	**FSS Antenna Response**	**Hybrid Antenna Response**	**Interpretation**
No object / Free space (air or empty surrounding near antenna)	Flat response	Flat response	No material or negligible interaction with EM field
High-conductivity material (e.g., copper, aluminum)	Return loss worsens, S-parameters degrade	Parameters remain stable	Clearly identifiable as a **conductor**
Low-loss dielectric (e.g., plastics, ceramics)	Minimal or no change	Shift in resonant frequency and/or return loss	Identified as **non-conductive dielectric**
Lossy or composite material (e.g., semi-conductive or moisture-containing media)	Irregular variation	Inconsistent or mixed response	Likely a **lossy or heterogeneous** material

This table can be used as a basic rule-set for classifying unknown materials using the simulated or measured S-parameter behavior of both antennas.

Summary

- The FSS-only antenna demonstrated poor robustness in the presence of conductors and low sensitivity to small dielectric changes.
- The hybrid FSS + SRR antenna provided:
  - High sensitivity to dielectric materials
  - Stable and consistent response to conductors
  - Distinct S-parameter shifts suitable for material classification
- Materials with higher dielectric constants exhibited slight downward shifts in the resonant frequency.
- The hybrid design lays a strong foundation for future development of non-contact material sensors.

References

[1] U. Singh, A. Ahmed, and J. Mukherjee, "Microstrip patch antenna as sensor based on metamaterial integrated structures for noninvasive characterization of biological materials," *IEEE Sensors Journal*, vol. 24, no. 7, pp. 9970–9981, 2024.

[2] M. Navarro-Cía, M. Beruete, F. Falcone, and M. Sorolla, "Novel metamaterials at millimeter and terahertz waves and lenses applications," in *2009 Asia Pacific Microwave Conference*, pp. 1289–1292, 2009.

[3] H. Nornikman, B. H. Ahmad, M. Z. A. Abd Aziz, and A. R. Othman, "Effect of single complimentary split ring resonator structure on microstrip patch antenna design," in *2012 IEEE Symposium on Wireless Technology and Applications (ISWTA)*, pp. 239–244, 2012.

[4] R. Mishra and A. Rai, "Effect of fss structure on planar patch antenna," in *2015 International Conference on Energy Economics and Environment (ICEEE)*, pp. 1–7, 2015.

[5] S. Arora and J. Mukherjee, "Rcs reduction of slot antenna using fss structures," in *2023 IEEE Microwaves, Antennas, and Propagation Conference (MAPCON)*, pp. 1–4, 2023.

Acknowledgements

I take this opportunity to acknowledge and express my gratitude to all those who supported and guided me during the dissertation work. I am grateful to the Almighty for the abundant grace and blessings that enabled me to complete this dissertation successfully.

Digital Signature
Pullabhotla Bhuvana Chandra
(200070063)
26-Jun-25 08:09:42 AM

Pullabhotla Bhuvana Chandra

Roll.No: 200070063

Date: 23-06-2025